

Measurement of $\gamma + c + \mathbf{X}$ and $\gamma + b + \mathbf{X}$ Production Cross Sections at $\sqrt{s} = 1.96$ TeV

Daniel Duggan

Florida State University

Abstract. The photon plus heavy-flavour quark (b, c) final state provides a unique and valuable window into both the sea quark content of the proton and the splitting of gluons into heavy-flavour quark pairs. A new combination of experimental techniques has provided the basis for the first measurements of the differential $\gamma + c + \mathbf{X}$ and $\gamma + b + \mathbf{X}$ production cross sections at $\sqrt{s} = 1.96$ TeV. The measurements use $\sim 1 \text{ fb}^{-1}$ of data from $p\bar{p}$ collisions collected with the DØ detector.

1. Introduction

The results presented are the first measurements of the differential $\gamma + c$ jet and $\gamma + b$ jet production cross sections at a hadron-hadron collider [1]. The measurements used $\sim 1 \text{ fb}^{-1}$ of data and were performed at the Fermilab Tevatron $p\bar{p}$ collider at $\sqrt{s} = 1.96$ TeV collected using the DØ detector. The presented production cross sections are differential with respect to the photon candidate's transverse momentum (p_T^γ) and are divided into five p_T^γ bins. The measurements are also differential with respect to the leading jet's rapidity (y^{jet}) and the leading photon's rapidity (y^γ) and are binned in two regions of photon-jet rapidities: $y^\gamma \cdot y^{\text{jet}} > 0$ and $y^{\text{jet}} \cdot y^\gamma < 0$.

2. Data Selection

Events are recorded using the DØ detector [2] and must contain at least one photon candidate and at least one heavy-flavour jet candidate. The photon and jet candidates with the highest transverse momenta (leading) are selected. The p_T of the photon candidate must be greater than 30 GeV/ c with $|y^\gamma| < 1.0$. The leading jet must satisfy $p_T > 15$ GeV/ c and $|y^{\text{jet}}| < 0.8$. The primary collision vertex must be located within 35 cm of the detector's center along the beam pipe, reconstructed with at least three associated tracks. To suppress background events coming from cosmic-ray muons and $W \rightarrow \ell\nu$ decays, the total missing transverse energy (E_T^{Miss}) in the event must satisfy the condition of $E_T^{\text{Miss}} < 0.7 \cdot p_T^\gamma$.

This analysis employs triggers that distinguish large depositions of energy in the electromagnetic (EM) calorimeter, and events are selected if at least one of these triggers has fired. The photon candidate is reconstructed, forming a cluster of energy. The reconstruction procedure sums the total energy deposited in the calorimeter within a cone of radius $\mathcal{R} = 0.2$, where $\mathcal{R} = \sqrt{(\Delta\eta)^2 + (\Delta\phi)^2}$. At least 96% of the photon candidate's energy must be in the EM calorimeter, and it must be spatially well isolated. To be considered isolated, the total energy in a cone of $\mathcal{R} = 0.4$, excluding the candidate's energy in the EM calorimeter (E_{EM}), must be less than 7% of E_{EM} . Additionally, the energy deposition within the third layer of the

EM calorimeter must be consistent with that of an electromagnetic shower. Photons traversing the DØ detector typically do not leave tracks, thus the photon candidate is required to have less than a 0.1% probability of being spatially matched to any track in the event. To reject additional backgrounds coming from dijet events, an artificial neural network (γ -ANN) [3] is used with the requirement of γ -ANN > 0.7 .

Jets are reconstructed using DØ's RunII algorithm [4] with a radius 0.5. The leading jet is subjected to the additional requirement of having at least two associated tracks with hits in the silicon tracker, one with $p_T > 1.0$ GeV/ c and the another with $p_T > 0.5$ GeV/ c . Heavy-flavour jets are identified using information arising from the long lifetimes of their hadrons. To best enhance the fraction of jets originating from heavy-flavour quarks, an artificial neural network (b -ANN) is employed. The b -ANN [5] is trained such that the output of heavy-flavour jets tends toward one and that of light (u , d , s quarks and gluons) jets tends to zero. For this selection, the requirement of b -ANN > 0.85 must be satisfied.

3. Purity Estimates

The fraction of direct photons in the final data sample is determined from a simultaneous fit of the γ -ANN output shape in data using templates derived from Monte Carlo (MC) signal photon and background dijet events simulated using PYTHIA [6]. The fitting procedure determines the linear combination of the signal and background templates that best describes the output shape in data. The fit is performed in each p_T^γ bin for both rapidity regions separately.

The fraction of c and b jets in the final data sample is determined using a similar method to that of photon purity technique. However, for the heavy-flavour fraction fitting technique, another discriminant, $P_{b\text{-jet}}$ was used. $P_{b\text{-jet}}$ is defined as $P_{b\text{-jet}} = -\ln \prod_i P_{\text{track}}^i$, where P_{track}^i is the probability of a track in the jet cone to originate from the primary collision vertex, omitting the least likely track to have come from this vertex. The value of $P_{b\text{-jet}}$ is large for b jets, and tends toward zero for light jets. The shape of the $P_{b\text{-jet}}$ distribution in data is fit from MC templates for both b jets and c jets, with the light jet template coming from a light jet enriched sample in data. The fit is performed in each p_T^γ bin separately, and the quality of the fit in each bin is of good quality. As an example, the result of the fit for $50 < p_T^\gamma < 70$ GeV/ c is shown in Fig. 1.

4. Cross Section Results

The measured differential cross sections are presented in five p_T^γ bins and two regions of $y^\gamma \cdot y^{\text{jet}}$, and can be seen in Fig. 2 for both the $\gamma + b$ and $\gamma + c$ processes. Due to the finite resolution of the calorimeter, p_T^γ smearing effects were accounted for using the unfolding method described in Ref. [7]. Statistical uncertainties for these results vary between 0.2% for $30 < p_T^\gamma < 40$ GeV/ c to $\sim 9\%$ for $90 < p_T^\gamma < 150$ GeV/ c , and the systematic uncertainties range from 15% to 28%. The theoretical predictions from next-to-leading (NLO) order calculations [8] are also presented in Fig. 2, where the renormalization scale μ_R , factorization scale μ_F and fragmentation scale μ_f are all set equal to p_T^γ .

The ratios of the measured to the predicted cross sections for both $\gamma + b$ and $\gamma + c$ cross sections in the two rapidity regions are shown in Fig. 3. The uncertainty due to the scale choice is estimated by simultaneously varying all three scales by a factor of two, $\mu_{R,F,f} = 0.5p_T^\gamma$ and $\mu_{R,F,f} = 2p_T^\gamma$. The CTEQ6.6M parton distribution functions (PDFs) were used in the theoretical calculations, and their corresponding uncertainties were calculated according to the prescription in Ref. [9]. Agreement within uncertainties can be seen in Fig. 3 for the $\gamma + b$ cross sections between data and theory in both rapidity regions. The $\gamma + c$ cross sections show agreement within uncertainties up to $p_T^\gamma \sim 70$ GeV/ c ; however, there is a rising discrepancy between data and theory that grows as p_T^γ increases. Certain models, including those that include an intrinsic charm (IC) component to the proton, predict higher cross sections for $\gamma + c$

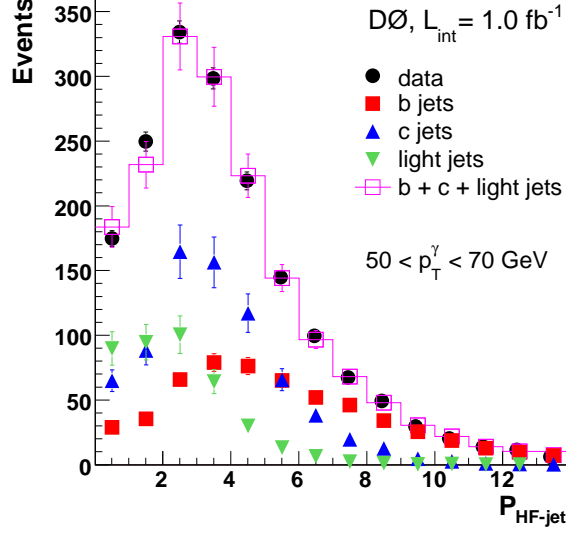


Figure 1. Distribution of the $P_{b\text{-jet}}$ discriminant in the final data sample in the range of $50 < p_T^\gamma < 70 \text{ GeV}/c$. The templates for light, c and b jets have been normalized to the number of events in data and then weighted by their found flavour fractions, and the shape of their sum is found to be in good agreement with that of the data. The shown uncertainties for the data are statistical in nature, whereas for the templates they incorporate statistical and fitting uncertainties.

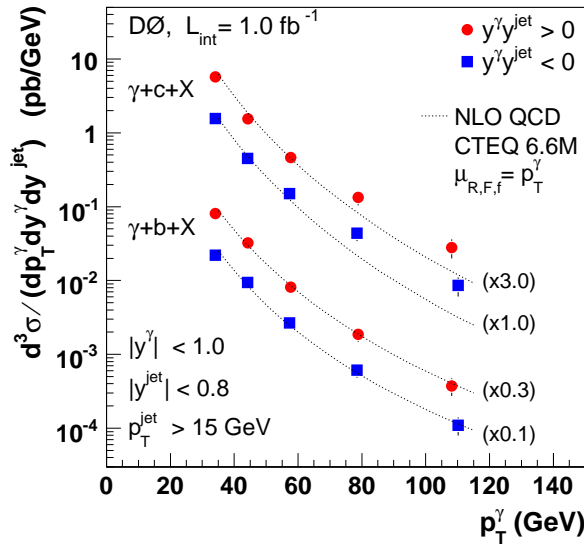


Figure 2. The $\gamma + b$ and $\gamma + c$ differential cross sections as a function of p_T^γ for both rapidity regions. The data points include the overall uncertainties from the measurement, and the theoretical predictions are displayed as dotted lines.

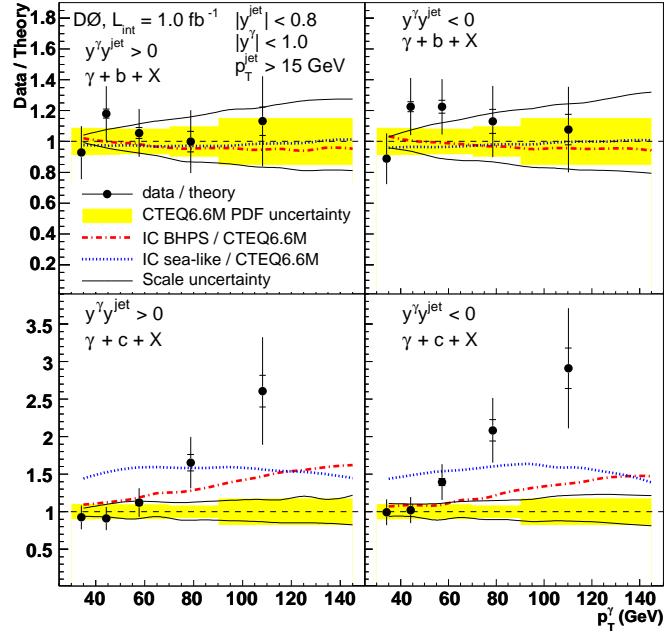


Figure 3. The ratios of the measured to the predicted cross sections for $\gamma + b$ production (top) and $\gamma + c$ production (bottom) in each rapidity region. The data points include both their statistical (inner tick) and overall uncertainties (entire error bar). The uncertainties from the theoretical predictions include those from the CTEQ 6.6M PDFs (yellow band) and from the choice of scale (full line). The ratio of two intrinsic charm models to the standard theoretical predictions are also included (dashed lines).

production. Although at least one IC model shows better agreement with the data than the standard theoretical predictions do, neither model shows agreement for the entire p_T^γ range in either rapidity region.

- [1] D0 Collaboration, V.M. Abazov *et al*, Phys. Rev. Lett. **102**, 192002 (2009).
- [2] D0 Collaboration, V.M. Abazov *et al*, Nucl. Instrum. Methods Phys. Res. A **565**, 463 (2006).
- [3] D0 Collaboration, V. Abazov *et al.*, Phys. Lett. B **666**, 435 (2008).
- [4] G.C. Blazey *et al.*, arXiv:hep-ex/0005012 (2000).
- [5] T. Scanlon, Ph.D. thesis, FERMILAB-THESIS-2006-43.
- [6] T. Sjostrand, Comput. Phys. Commun. **135**, 238 (2001).
- [7] B. Abbott *et al* (D0 Collaboration), Phys. Rev. D **64**, 032003 (2001).
- [8] T. Stavreva, J.F. Owens, arXiv:0901.3791v1 (2009).
- [9] D. Stump *et al.*, JHEP **0310**, 046 (2003).